

A Poly-Si-Based Vertical Comb-Drive Two-Axis Gimbaled Scanner for Optical Applications

Mingching Wu, Hung-Yi Lin, and Weileun Fang

Abstract—This work presents a novel two-axis gimbaled mirror for optical scanning applications. This scanner has been implemented using the molded surface-micromachining and bulk etching release (MOSBE II) process. Thus, the vertical comb-drive actuators are employed to realize the large stroke. The thin-film electrical routings are employed to drive the actuators individually. The rib-reinforced structures are exploited to increase the stiffness of mirror plate and supporting frame. In addition, the moving space created by backside deep reactive ion etching enables the mirror to perform large out-of-plane angular motion. The measured radius of curvature of reinforced mirror plate is 0.43 m. The maximum scanning angle of two driving axis are $\pm 3.8^\circ$ at 55 V and $\pm 2.4^\circ$ at 100 V, respectively. The resonant frequencies associated with the scanning modes are 5.8 and 7.8 kHz, respectively. In addition, the two-dimensional scanning images such as Lissajous patterns are also demonstrated.

Index Terms—Comb drive, microelectromechanical systems (MEMS), micromirror, MOSBE platform, poly-Si micromachining, reinforced structure.

I. INTRODUCTION

THE TWO-AXIS gimbaled scanning mirror, which employs microactuators to independently manipulate incident light in two orthogonal directions, is a key enabling component for optical applications [1], [2]. To achieve the desired performances, including large scanning angle, angular accuracy, high frequency response, and low driving voltages, the design and fabrication of two-axis microelectromechanical systems (MEMS) scanning mirror become the challenge for the state-of-the-art. Particularly, the scanner design is highly related with implemented fabrication process.

The two poly-Si multiuser MEMS process (MUMPs) is the most popular fabrication technology to not only fabricate but also integrate micromachined components. The two poly-Si scanner in [3] employs gap-closing actuators underneath the mirror plate for two-axis scanning. However, the thin-film mirror plate will be deformed by residual stress due to the small stiffness [4]. The large moving space is available for MUMPs scanner under the assistant of a self-assembly mechanism, yet the stability problem during operation cannot be ignored [3]. In addition, the pull-in phenomenon limits the controllable angle of the scanning mirror in the meantime [5]. To implement microoptical devices on the

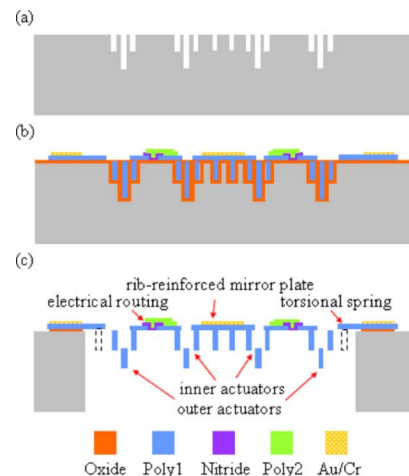


Fig. 1. Concept of MOSBE II processes with deep silicon etching, thin-film depositions, and bulk silicon etching.

single-crystal silicon (SCS) is regarded as a superior approach due to the large thickness and the mirror flat surface provided by SCS. Thus, the gimbaled mirror driven by gap-closing actuators has been successfully demonstrated by the silicon-on-insulator (SOI) process and bonding techniques [6]. The thicker mirror plate substantially improves the optical quality of the scanner. In addition, the vertical comb-drive actuator to provide a large stroke with low driving voltages for the optical scanner has also been demonstrated by the SOI process [7].

In summary, the existing two-axis MEMS scanner has the following design considerations: First, the mirror plate should be light and rigid to provide high resonant frequency and flat optical surface. Second, the actuator should allow the scanner to have a large angular displacement and a small driving voltage. Third, the electrical routing should be considered for both single- and dual-axis scanning. This work designs a novel two-axis scanning mirror, and further employs the MUMPs compatible molded surface-micromachining and bulk etching release (MOSBE II) process [8] to implement the device.

II. DESIGN AND FABRICATION

Fig. 1 indicates the concept of the MOSBE II process. Briefly, trenches of two different depths are defined by deep reactive ion etching (DRIE) [Fig. 1(a)]. The first poly-Si (poly1) film can refill the trenches to form microstructures with various thicknesses [Fig. 1(b)]. In addition, the second poly-Si (poly2) film is exploited to act as the electrical routing. Finally, the front-side DRIE is used to partially remove the poly-Si so as to allow the structure locating at different vertical positions [Fig. 1(c)]. The backside DRIE is employed to release the device, and provide a large moving space as well.

Manuscript received December 22, 2005; revised July 3, 2006.

M. Wu is with the Department of Power Mechanical Engineering, National Tsing Hua University, Hsinchu 300, Taiwan, R.O.C.

H.-Y. Lin is with the Touch Microsystem Technology Inc., Taoyuan 326, Taiwan, R.O.C.

W. Fang is with the Department of Power Mechanical Engineering, National Tsing Hua University, Hsinchu 300, Taiwan, R.O.C. (e-mail: fang@pme.nthu.edu.tw).

Color versions of Figs. 1–6 are available online at <http://ieeexplore.ieee.org>.
Digital Object Identifier 10.1109/LPT.2006.883251

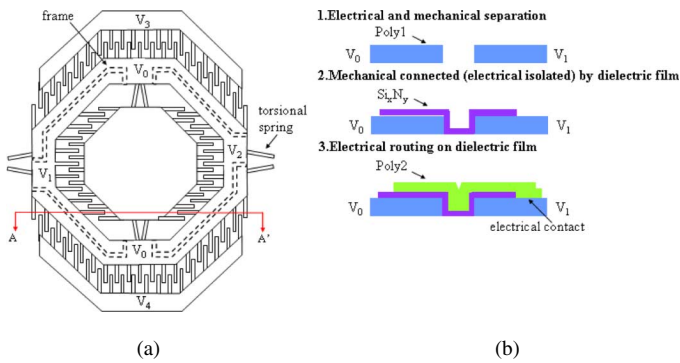


Fig. 2. Schematic illustrations of (a) the top view of the proposed two-axis scanner, and (b) the process steps for electrical routing and isolation.

Fig. 2 indicates the design of the proposed two-axis gimbaled scanner and the cross section of AA' is shown in Fig. 1(c). The gimbaled scanner consists of V-shaped torsional springs, rib-reinforced structures, vertical comb-drive actuators, electrical routings, and motion cavity. These mechanical and electrical components are made of poly1 and poly2 films. The V-shape torsional spring can improve the stability of vertical comb-drive actuators [9]. The thick trench-refilled structure in Fig. 1(b) is exploited to act as a torsional spring. Therefore, the high aspect ratio spring has large bending stiffness to prevent wobble motion. Since the width of the spring remains small, it has small torsional stiffness and is easy to be twisted. The thin-film poly-Si structures usually experience some unwanted deformations resulted from the residual stresses after fabrication and the inertia force during operation. The reinforced ribs are employed to significantly increase the stiffness of the mirror plate and supporting frames. Thus, the flatness of the mirror plate and dynamic stability of the scanner are improved.

For the two-axis scanning application, the vertical comb electrodes are distributed along the boundaries of the mirror plate and supporting frames. According to the MOSBE II process, the stationary and moving electrodes are perfectly aligned by photolithography [9]. In order to operate the vertical comb actuators independently, the scanner has five electrical potential regions ($V_0 \sim V_4$), as indicated in Fig. 2. The inner supporting frame (poly1) is first etched into various separate regions. These regions are disconnected mechanically and electrically. After depositing with insulation layer (Si_3N_4), these separate regions are connected with each other mechanically. However, the electrical potentials of these regions remain independent. Finally, the poly2 film is employed to act as the electrical routing to define the potential of these regions. Therefore, the vertical comb drive actuators, which drive the mirror plate and inner frame independently, could route the electrical potential through the torsional spring to provide two-axis operation.

III. RESULTS AND TESTING

The typical fabricated two-axis scanning mirror is successfully demonstrated in Fig. 3. The inner and outer vertical comb-drive actuators, supporting frames, V-shape torsional springs, and rib-reinforced mirror plate are clearly observed from the scanning electron microscope (SEM) photograph. The scanning mirror is suspended above a micromachined cavity by the torsional springs. The SEM photograph of Fig. 4(a) shows the

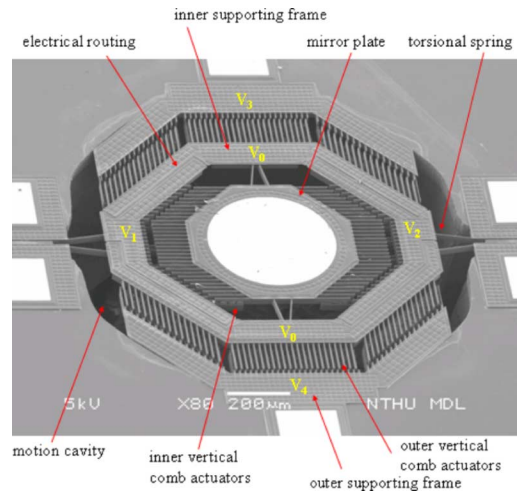


Fig. 3. SEM photograph of a typical fabricated two-axis scanner; the key components are also indicated in the figure.

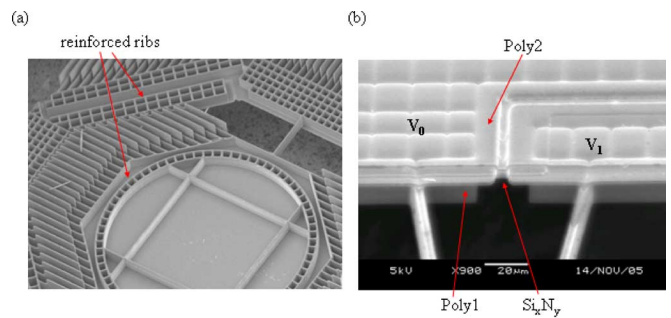


Fig. 4. Zoom in SEM photograph of the scanner in Fig. 3. (a) Reinforced ribs on the backside of mirror plate and frame and (b) the electrical routing and isolation.

backside of the scanner, the reinforced ribs distributed on the mirror plate and supporting frames are clearly observed. In this case, the trench-refilled reinforced ribs were $20 \mu\text{m}$ thick. The SEM photograph in Fig. 4(b) indicates the electrical routing and insulation on the supporting frame. Thus, the electrically independent potentials could be routing through the torsional spring to provide two-axis operation.

The static and dynamic behaviors of the optical scanner shown in Fig. 3 were characterized to demonstrate the performance of proposed design. During the static test, a dc voltage was applied to the vertical comb actuator to drive the mirror. Meanwhile, the radius of curvature (ROC) and the angular deflection of the scanner were characterized by a commercial optical interferometer system. The measured ROC of the mirror plate was 0.43 m and the corresponding optical magnification ratio is 1.31 (the magnification ratio of an ideal flat mirror is 1). As a comparison, the $2\text{-}\mu\text{m}$ -thick poly-Si mirror in [4], [9], and [10] has an ROC of $<20 \text{ mm}$, and the $22.5\text{-}\mu\text{m}$ -thick SOI mirror in [10] has an ROC of 2.65 m. Moreover, the ROC of the rib-reinforced scanner in [8] was 0.15 m since it had a lower number of reinforced ribs around the rim of the mirror. Thus, the reinforced ribs did significantly increase the stiffness of the structure, and the optical property of the mirror plate has been improved. The peaks on surface topology are marks of the reinforced ribs.

The angular motion of the mirror versus the dc driving voltage was also characterized using the optical interferometer. The measurement results are shown in Fig. 5(a). Hence,

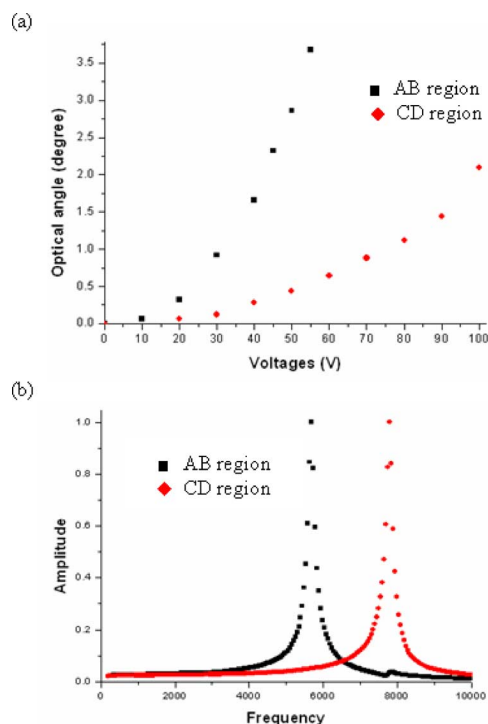


Fig. 5. Driving test of the mirror. (a) Variation of the driving voltage and the angular displacement of the mirror determined from the optical interferometer, and (b) the frequency response determined from the LDV.

the mirror plate had a maximum scanning angle of 3.8° at 55 V when applying voltages on inner comb actuators. The maximum scanning angle of mirror was 2.4° at 100 V when driving at outer comb actuators. The corresponding optical resolution is 155 pixels per line in $\pm 3.8^\circ$ scanning angle (the ideal flat mirror is 204 pixels per line). During the dynamic behaviors test, an ac voltage was applied to the inner and outer vertical comb actuators for two-axis scanning. The optical Laser Doppler Vibrometer (LDV) was used to characterize the dynamic response of the scanner. Fig. 5(b) shows a typical measured frequency response of the scanner when driving at inner and outer comb actuators, respectively. A sinusoidal driving signal with an amplitude of ± 10 V and a dc-bias of 10 V was employed to excite the inner and outer actuators. The measured results show that the first torsional vibration mode about y -axis is 5.8 kHz and the corresponding quality factor is 40. This vibration mode enables an incident laser beam to have a large scan angle in the x -axis (horizontal). On the other hand, the first resonant frequency is 7.8 kHz for a large y -axis (vertical) scanning angle.

The scanning images in Fig. 6 result from the laser spot reflected from the scanner in Fig. 3. The large one-dimensional (1-D) scanning lines, as shown in Fig. 6(a) and (b), were, respectively, reflected from the scanner driven at horizontal and vertical scanning modes. Fig. 6(c) shows the large two-dimensional (2-D) scan image when both horizontal and vertical scanning modes were excited. The Lissajous pattern in Fig. 6(d) is resulted from the scanner when its inner and outer actuators driven at a frequency ratio of 4 ($f_{\text{vertical}}/f_{\text{horizontal}} = 4$). These 1-D and 2-D scanning images demonstrate that the present electrical routing approach allows the inner and outer actuators to be driven individually as well as simultaneously.

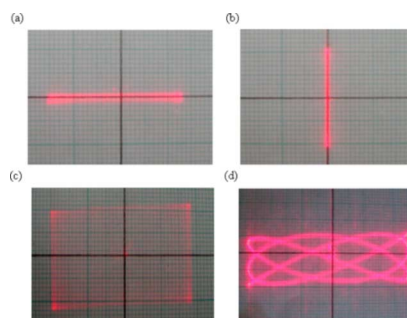


Fig. 6. Scanning images and Lissajous patterns of the reflected laser spot from the two-axis scanner. (a) Horizontally scanning line, (b) vertically scanning line, (c) 2-D scanning image, and (d) $f_{\text{vertical}}/f_{\text{horizontal}} = 4$.

IV. CONCLUSION

This work presents the design, fabrication, and characterization of a novel two-axis scanning mirror. The stiffness of mirror and supporting frames has been significantly increased by reinforced ribs. The ROC of the mirror plate is improved by rib-reinforced structures and reached 0.43 m for good reflectivity surface. The vertical comb actuators enable the scanner a large stroke. The electrical routing and insulation are available by poly-Si and Si_xN_y multilayers. Thus, the electrically independent potentials could be routing through the torsional bar to provide two-axis operation. The moving space created by backside DRIE etching enables the mirror to perform large out-of-plane motion. In addition, the respective resonant frequencies of two driving axis are 5.8 and 7.8 kHz. The frequency is high enough to prevent the disturbance of environment and provide highly operated speed. In applications, various 1-D and 2-D scanning images have been demonstrated.

REFERENCES

- [1] V. A. Aksyuk, F. Pardo, D. Carr, D. Greywall, H. B. Chan, M. E. Simon, A. Gasparyan, H. Shea, V. Lifton, C. Bolle, S. Arney, R. Frahm, M. Paczkowski, M. Haueis, R. Ryf, D. T. Neilson, J. Kim, C. R. Giles, and D. Bishop, "Beam-steering micromirrors for large optical cross-connects," *J. Lightw. Technol.*, vol. 21, no. 3, pp. 634–642, Mar. 2003.
- [2] H. Urey, F. DeWitt, P. Lopez, and J. Tauscher, "MEMS raster correction scanner for SXGA resolution retinal scanning display," *Proc. SPIE*, vol. 4985, pp. 106–114, 2003.
- [3] V. A. Aksyuk, F. Pardo, and D. J. Bishop, "Stress-induced curvature engineering in surface-micromachined devices," *Proc. SPIE*, vol. 3680, pp. 984–993, 1999.
- [4] L. Y. Lin, E. L. Goldstein, and R. W. Tkach, "On the expandability of free-space micromachined optical cross connects," *J. Lightw. Technol.*, vol. 18, no. 4, pp. 482–489, Apr. 2000.
- [5] O. Degani, E. Socher, A. Lipson, T. Lejtner, D. J. Setter, S. Kaldor, and Y. Nemirovsky, "Pull-in study of an electrostatic torsion microactuator," *J. Microelectromech. Syst.*, vol. 7, no. 4, pp. 373–379, Dec. 1998.
- [6] D. S. Greywall, P. A. Busch, F. Pardo, D. W. Carr, G. Bogart, and H. T. Soh, "Crystalline silicon tilting mirrors for optical cross-connect switches," *J. Microelectromech. Syst.*, vol. 12, no. 5, pp. 708–712, Oct. 2003.
- [7] R. A. Conant, J. T. Nee, K. Lau, and R. S. Mueller, "A fat high-frequency scanning micromirror," in *Proc. Solid-State Sensor and Actuator Workshop*, Hilton Head, SC, 2000, pp. 6–9.
- [8] M. Wu and W. Fang, "Design and fabrication of MEMS devices using the integration of MUMPs, trench-refilled molding, DRIE and bulk silicon etching processes," *J. Micromech. Microeng.*, vol. 15, pp. 535–542, 2005.
- [9] O. Tsuboi, Y. Mizuno, N. Koma, H. Soneda, H. Okuda, S. Ueda, I. Sawaki, and F. Yamagishi, "A rotational comb-driven micromirror with a large deflection angle and low drive voltage," in *Proc. IEEE MEMS'02*, Las Vegas, NV, Jan. 2002, pp. 532–535.
- [10] G.-D. J. Su, H. Nguyen, P. Paterson, H. Toshiyoshi, and M. C. Wu, "Surface-micromachined 2-D optical scanners with high-performance single-crystalline silicon micromirrors," *IEEE Photon. Technol. Lett.*, vol. 13, no. 6, pp. 606–608, Jun. 2001.